

# Loss-compensated and active hyperbolic metamaterials

Xingjie Ni,<sup>1</sup> Satoshi Ishii,<sup>1</sup> Mark D. Thoreson,<sup>1</sup> Vladimir M. Shalaev,<sup>1</sup> Seunghoon Han,<sup>2</sup>  
Sangyoon Lee,<sup>2</sup> and Alexander V. Kildishev<sup>1,\*</sup>

<sup>1</sup>*Birck Nanotechnology Center, School of Electrical and Computer Engineering, Purdue University, West Lafayette, IN 47907, USA*

<sup>2</sup>*Samsung Advanced Institute of Technology, Samsung Electronics, Yongin, Gyeonggi-do 446-712, South Korea*  
*\*kildishev@purdue.edu*

**Abstract:** We have studied the dispersion relations of multilayers of silver and a dye-doped dielectric using four methods: standard effective-medium theory (EMT), nonlocal-effect-corrected EMT, nonlinear equations based on the eigenmode method, and a spatial harmonic analysis method. We compare the validity of these methods and show that metallic losses can be greatly compensated by saturated gain. Two realizable applications are also proposed. Loss-compensated metal-dielectric multilayers that have hyperbolic dispersion relationships are beneficial for numerous applications such as subwavelength imaging and quantum optics.

©2011 Optical Society of America

**OCIS codes:** (160.3918) Metamaterials; (160.1190) Anisotropic optical materials.

---

## References and links

1. R. Wangberg, J. Elser, E. E. Narimanov, and V. A. Podolskiy, "Nonmagnetic nanocomposites for optical and infrared negative-refractive-index media," *J. Opt. Soc. Am. B* **23**(3), 498–505 (2006).
2. A. J. Hoffman, L. Alekseyev, S. S. Howard, K. J. Franz, D. Wasserman, V. A. Podolskiy, E. E. Narimanov, D. L. Sivco, and C. Gmachl, "Negative refraction in semiconductor metamaterials," *Nat. Mater.* **6**(12), 946–950 (2007).
3. M. Silveirinha and N. Engheta, "Tunneling of electromagnetic energy through subwavelength channels and bends using epsilon-near-zero materials," *Phys. Rev. Lett.* **97**(15), 157403 (2006).
4. A. Alù, M. Silveirinha, A. Salandrino, and N. Engheta, "Epsilon-near-zero metamaterials and electromagnetic sources: Tailoring the radiation phase pattern," *Phys. Rev. B* **75**(15), 155410 (2007).
5. D. O. S. Melville and R. J. Blaikie, "Experimental comparison of resolution and pattern fidelity in single- and double-layer planar lens lithography," *J. Opt. Soc. Am. B* **23**(3), 461–467 (2006).
6. B. Wood, J. B. Pendry, and D. P. Tsai, "Directed subwavelength imaging using a layered metal-dielectric system," *Phys. Rev. B* **74**(11), 115116 (2006).
7. Z. Jacob, L. V. Alekseyev, and E. Narimanov, "Optical Hyperlens: Far-field imaging beyond the diffraction limit," *Opt. Express* **14**(18), 8247–8256 (2006).
8. A. Salandrino and N. Engheta, "Far-field subdiffraction optical microscopy using metamaterial crystals: Theory and simulations," *Phys. Rev. B* **74**(7), 075103 (2006).
9. Z. Liu, H. Lee, Y. Xiong, C. Sun, and X. Zhang, "Far-field optical hyperlens magnifying sub-diffraction-limited objects," *Science* **315**(5819), 1686 (2007).
10. I. I. Smolyaninov, Y. J. Hung, and C. C. Davis, "Magnifying superlens in the visible frequency range," *Science* **315**(5819), 1699–1701 (2007).
11. Z. Jacob, J. Y. Kim, G. V. Naik, A. Boltasseva, E. Narimanov, and V. M. Shalaev, "Engineering photonic density of states using metamaterials," *Appl. Phys. B-Lasers Opt.* **1**, 264 (2010).
12. E. Narimanov, M. A. Noginov, H. Li, and Y. Barnakov, "Darker than black: Radiation-absorbing metamaterial," in *Quantum Electronics and Laser Science Conference*, (Optical Society of America, 2010).
13. Z. Jacob, I. Smolyaninov, and E. Narimanov, "Single photon gun: Radiative decay engineering with metamaterials," in *CLEO/QELS*, (Optical Society of America, 2009).
14. N. Mattiucci, G. D'Aguzzo, M. Scalora, M. J. Bloemer, and C. Sibilia, "Transmission function properties for multi-layered structures: application to super-resolution," *Opt. Express* **17**(20), 17517–17529 (2009).
15. P. West, S. Ishii, G. Naik, N. Emani, V. M. Shalaev, and A. Boltasseva, "Searching for better plasmonic materials," *Laser Photon. Rev.* **4**, 765–808 (2009).
16. M. J. Bloemer, G. D'Aguzzo, M. Scalora, N. Mattiucci, and D. de Ceglia, "Energy considerations for a superlens based on metal/dielectric multilayers," *Opt. Express* **16**(23), 19342–19353 (2008).

17. J. Zhang, H. Jiang, B. Gralak, S. Enoch, G. Tayeb, and M. Lequime, "Compensation of loss to approach-1 effective index by gain in metal-dielectric stacks," *Eur. Phys. J. Appl. Phys.* **46**(3), 32603 (2009).
18. S. Xiao, V. P. Drachev, A. V. Kildishev, X. Ni, U. K. Chettiar, H. K. Yuan, and V. M. Shalaev, "Loss-free and active optical negative-index metamaterials," *Nature* **466**(7307), 735–738 (2010).
19. M. P. H. Andresen, A. V. Skaldebo, M. W. Haakestad, H. E. Krogstad, and J. Skaar, "Effect of gain saturation in a gain compensated perfect lens," *J. Opt. Soc. Am. B* **27**(8), 1610–1616 (2010).
20. J. Seidel, S. Grafström, and L. Eng, "Stimulated emission of surface plasmons at the interface between a silver film and an optically pumped dye solution," *Phys. Rev. Lett.* **94**(17), 177401 (2005).
21. M. A. Noginov, G. Zhu, M. Bahoura, J. Adegoke, C. E. Small, B. A. Ritzo, V. P. Drachev, and V. M. Shalaev, "Enhancement of surface plasmons in an Ag aggregate by optical gain in a dielectric medium," *Opt. Lett.* **31**(20), 3022–3024 (2006).
22. I. De Leon and P. Berini, "Amplification of long-range surface plasmons by a dipolar gain medium," *Nat. Photonics* **4**(6), 382–387 (2010).
23. T. Tumkur, G. Zhu, P. Black, Y. A. Barnakov, C. E. Bonner, and M. A. Noginov, "Control of spontaneous emission with functionalized multilayered hyperbolic metamaterials," in *SPIE*, (San Diego, California, USA, 2011), p. 809300.
24. P. Yeh, *Optical Waves in Layered Media* (Wiley-Interscience, 2005).
25. J. Elser, V. A. Podolskiy, I. Salakhutdinov, and I. Avrutsky, "Nonlocal effects in effective-medium response of nanolayered metamaterials," *Appl. Phys. Lett.* **90**(19), 191109 (2007).
26. X. Ni, Z. Liu, A. Boltasseva, and A. V. Kildishev, "The validation of the parallel three-dimensional solver for analysis of optical plasmonic bi-periodic multilayer nanostructures," *Appl. Phys. A-Mater.* **100**, 365–374 (2010).
27. Z. Liu, K. P. Chen, X. Ni, V. P. Drachev, V. M. Shalaev, and A. V. Kildishev, "Experimental verification of two-dimensional spatial harmonic analysis at oblique light incidence," *J. Opt. Soc. Am. B* **27**(12), 2465–2470 (2010).
28. S. Thongrattanasiri and V. A. Podolskiy, "Hypergratings: nanophotonics in planar anisotropic metamaterials," *Opt. Lett.* **34**(7), 890–892 (2009).
29. W. Chen, M. D. Thoreson, S. Ishii, A. V. Kildishev, and V. M. Shalaev, "Ultra-thin ultra-smooth and low-loss silver films on a germanium wetting layer," *Opt. Express* **18**(5), 5124–5134 (2010).
30. X. Ni, Z. Liu, and A. V. Kildishev, "PhotonicsDB: Optical constants," (2008). doi:10254/nanohub-r3692.10.
31. P. B. Johnson and R. W. Christy, "Optical constants of the noble metals," *Phys. Rev. B* **6**(12), 4370–4379 (1972).
32. Z. Liu, K.-P. Chen, X. Ni, V. P. Drachev, V. M. Shalaev, and A. V. Kildishev, "Experimental verification of two-dimensional spatial harmonic analysis at oblique light incidence," *J. Opt. Soc. Am. B* **27**(12), 2465–2470 (2010).
33. Y. Sivan, S. M. Xiao, U. K. Chettiar, A. V. Kildishev, and V. M. Shalaev, "Frequency-domain simulations of a negative-index material with embedded gain," *Opt. Express* **17**(26), 24060–24074 (2009).
34. V. C. Nguyen, L. Chen, and K. Halterman, "Total transmission and total reflection by zero index metamaterials with defects," *Phys. Rev. Lett.* **105**(23), 233908 (2010).
35. S. M. Feng and K. Halterman, "Parametrically shielding electromagnetic fields by nonlinear metamaterials," *Phys. Rev. Lett.* **100**(6), 063901 (2008).
36. A. Ciattoni, C. Rizza, and E. Palange, "Transmissivity directional hysteresis of a nonlinear metamaterial slab with very small linear permittivity," *Opt. Lett.* **35**(13), 2130–2132 (2010).
37. C. Rizza, A. Ciattoni, and E. Palange, "Two-peaked and flat-top perfect bright solitons in nonlinear metamaterials with epsilon near zero," *Phys. Rev. A* **83**(5), 053805 (2011).
38. P. Yeh, *Optical Waves in Layered Media* (John Wiley & Sons, Inc., Hoboken, NJ, 1988).
39. A. V. Kildishev and U. K. Chettiar, "Cascading optical negative index metamaterials," *Appl. Comput. Electrom.* **22**, 172 (2007).
40. X. Ni, Z. Liu, F. Gu, M. G. Pacheco, J. Borneman, and A. V. Kildishev, "PhotonicsSHA-2D: Modeling of single-period multilayer optical gratings and metamaterials," (2011). doi:10254/nanohub-r6977.12.

---

## 1. Introduction

Scientific interest in metal-dielectric multilayers has increased in recent years, due in part to the new and related ideas of metamaterials and transformation optics. Created from extremely thin, alternating layers of a metal (with a negative real permittivity) and a dielectric (with a positive real permittivity), metal-dielectric multilayer structures can provide truly unique optical properties that can be useful for a number of advanced applications and devices. The optical properties (permittivity, for instance) of multilayer structures can be strikingly different than those of natural materials, including natural crystals. In multilayer systems, we can obtain a hyperbolic dispersion relationship in which the permittivity along one axis is negative while the permittivities along the other axes are positive [1]. The applications of such an unusual material, called a hyperbolic metamaterial or HMM, include negative refraction [2], epsilon-near-zero (ENZ) materials [3, 4], superlenses [5, 6] and hyperlenses [7–10],

quantum optics [11], and many others [12–14]. One significant drawback of a passive optical HMM is that the intrinsic loss in the metal always limits the overall functionality [15, 16]. This is a fundamental challenge in the applications of HMMs, but it can be overcome by including active (gain) media in the system [17–19]. So far, gain media have been experimentally incorporated into various kinds of plasmonic and metamaterial systems including surface plasmon polaritons [20], localized surface plasmon polaritons [21], plasmonic waveguides [22], and negative index materials [18]. Incorporating gain within the multilayer system allows for the compensation of the metallic loss [23]. In fact, some experiments on metamaterials have even shown complete loss compensation or even overcompensation [18]. With gain, then, metal-dielectric HMM applications can be far more robust than with passive HMMs.

In Section 2 we model a metal-dielectric HMM for the case when the dielectric is an active medium, and we study the dispersion relationship of such a system. The cross section of a binary HMM, which consists of isotropic metal and dielectric layers, is schematically shown in Fig. 1. The permittivity and thickness of each layer are denoted respectively as  $\epsilon_j$  and  $\delta_j$ , where  $j=1$  for the metal layer and  $j=2$  for the dielectric layer, and the period of the structure is  $\delta = \delta_1 + \delta_2$ . We also define a linearly polarized plane wave with the following free-space parameters: wavelength  $\lambda$ , wavenumber  $k_0 = 2\pi/\lambda$ , and wavevector  $\mathbf{k}_0 = k_0(\hat{\mathbf{x}}\cos\theta + \hat{\mathbf{y}}\sin\theta)$ , where a given angle of incidence  $\theta$  is aligned with the structure ( $0 < \theta < \pi/2$ ). As discussed above, HMMs made from thin, alternating layers of a metal and a dielectric can be considered to be metamaterials as long as their periodicity  $\delta$  is significantly smaller than the free-space wavelength of the incident light ( $\lambda$ ), or more precisely, when  $k_0\delta \ll 1$ .

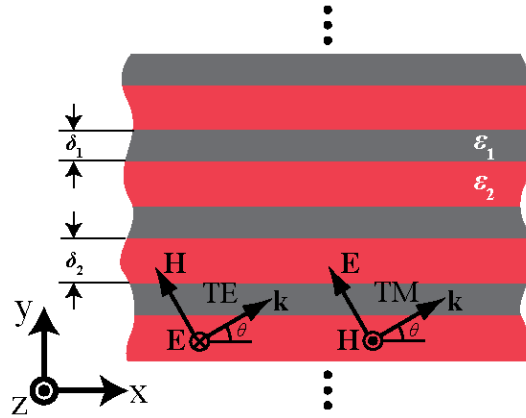


Fig. 1. Geometry of a metal-dielectric multilayer composite. The permittivities of the metal and dielectric layers are denoted respectively as  $\epsilon_1$  and  $\epsilon_2$ , and the thicknesses are  $\delta_1$  and  $\delta_2$ . All the layers are parallel to the  $x$ - $z$  plane.

When studying the dispersion relationships of multilayers, using T-matrices to form a set of nonlinear equations (NLE) is a rigorous method, and the resulting solutions are exact [24]. A simpler way is to use the standard effective medium theory (denoted as EMT<sub>1</sub> in this paper). The effective medium theory homogenizes the multilayers, thus giving the effective dielectric constants of the medium as a whole. A more advanced EMT method (denoted EMT<sub>2</sub>) [25] takes into account the nonlocal effects that are neglected in EMT<sub>1</sub>. With regard to numerical methods, spatial harmonic analysis (SHA) is a robust method to study periodic systems [26, 27]. All the details of the four methods discussed here are given in the addendum. We have tested these four different methods to model active HMMs and have

compared the results. In Section 3 we consider two realizable examples as possible applications of active HMMs: one is a hypergrating [28], and the other is an ENZ material.

## 2. Examples and discussion

In this section we estimate the properties of metal-dielectric multilayers by using the above-mentioned methods. We take silver as the material in all the metal layers. Note that thin silver films tend to form islands below 20 nm on a silica surface, which is not suitable for obtaining a multilayer structure. Recent studies have shown that a silver film evaporated on a 1-nm-thick germanium layer is continuous and smooth even at a 5-nm Ag thickness [29]. In our calculations, we used realistic values of the optical properties of the materials; these values are taken from experimental results. We take the permittivity of silver from [30], which uses a Drude-Lorentz model with 3 Lorentz terms. The parameters are fitted using measured data from [31]. The loss factor (a multiple of the collision rate in the Drude term) is set to two in order to take into account the size-dependent silver loss [32]. Since annealing can reduce the loss of germanium to negligible levels in the red part of the spectrum, which is our region of interest, the germanium layer is not modeled in our simulations. For the active dielectric medium, we take the gain values extracted from experimentally measured data of an organic dye (Rh800) mixed in epoxy [18, 33]. Typically, organic dyes mixed with polymers have high gain coefficients and have the advantage that they can be incorporated into any arbitrarily shaped spaces [18]. The refractive index of epoxy is 1.65, and the emission peak of Rh800 occurs at about 720 nm. Because the gain coefficient of a material is proportional to the imaginary part of the refractive index, we therefore modeled the active dielectric with a complex dielectric function. The imaginary part of the dielectric function is plotted in Fig. 2. Note that the real part of the dielectric function is not plotted here since it is dominated by the permittivity of the epoxy and is almost constant in this wavelength range. To simplify our modeling, we assumed that the active medium was operating in the saturated regime, and we hence neglected the time dependence of gain saturation.

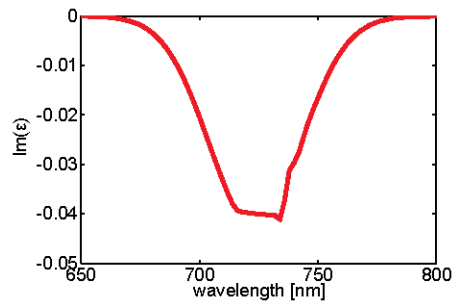


Fig. 2. Extracted imaginary part of the dielectric function of dye-doped epoxy. Note that the real part of the dielectric function (not shown) is dominated by the permittivity of the epoxy, which is about 2.72.

As an example system, we take a silver-gain multilayer structure consisting of alternating 20-nm-thick silver layers and 40-nm-thick gain layers. In Fig. 3 we plot the effective anisotropic permittivity of the structure calculated from the four methods (EMT<sub>1</sub>, EMT<sub>2</sub>, NLE, and SHA). The incidence angle ( $\theta$ ) is zero for the plot. Within the plotted wavelength range (650 – 800 nm), all four methods show that the multilayer has opposite signs for  $\epsilon_x$  and  $\epsilon_y$ , and it therefore exhibits hyperbolic dispersion.

It is also shown in Fig. 3 that the effective permittivity resulting from NLE and SHA are perfectly matched in both the x and y directions. This is not surprising, as both methods are aimed at calculating the eigenvalues of the composite layer and differ only in their numerical realizations. The results from EMT<sub>2</sub> are very close to those values. However, there are significant discrepancies between the results from EMT<sub>1</sub> and those from the other methods.

The relative errors are calculated using the results from SHA as the reference (exact value) using  $|(\varepsilon_{\text{calc}} - \varepsilon_{\text{SHA}}) / \varepsilon_{\text{SHA}}| \times 100\%$ . Comparing with EMT<sub>1</sub>, EMT<sub>2</sub> is more accurate and has lower error over the calculated wavelength range (the EMT<sub>2</sub> error is less than 3% in this case). We also note that the relative errors of the imaginary parts of the permittivities from both EMT<sub>1</sub> and EMT<sub>2</sub> are higher in the active region, which can be observed from the relative error plots in Fig. 3.

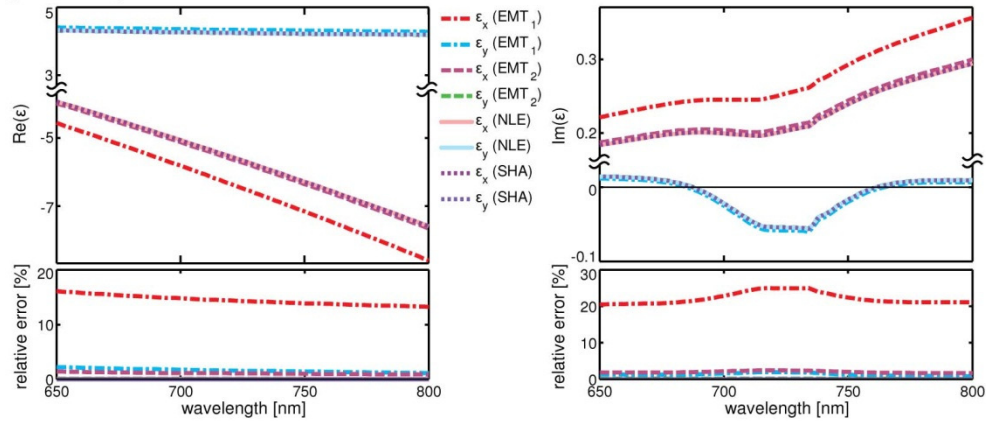


Fig. 3. Wavelength dependence of the effective anisotropic permittivity for the silver-gain HMM at normal incidence ( $\theta = 0$ ) calculated from EMT<sub>1</sub> (dashed-dotted line), EMT<sub>2</sub> (dashed line), NLE (solid line), and SHA (dotted line). Top left panel: the real part of the effective permittivity. Top right: the imaginary part of effective permittivity. Bottom panels: relative errors in percent with respect to the SHA results. Note that the results from NLE and SHA are coincident, and their curves are overlapping. The real part of permittivity in the y direction from EMT<sub>2</sub> is overlaps with the NLE and SHA curves (therefore it is obscured by the NLE and SHA curves and is not seen in the figure), and the rest of the EMT<sub>2</sub> curve partially overlaps with the NLE and SHA curves.

If we take a look at the fundamental mode for a TM-polarized wave propagating in the x direction in the structure, the real part of the modal index, which is  $\sqrt{\varepsilon_y}$ , is higher than the refractive index of the dielectric in the multilayer. This indicates that the dominant propagating mode is indeed a plasmonic mode. The imaginary part of the modal index, which has the same sign as  $\text{Im}(\varepsilon_y)$ , is negative from 700 nm to 750 nm. Within this range, the propagating TM wave is loss-free. However, in the x direction, we can see that the imaginary part of  $\varepsilon_x$  stays positive, which means that the loss is not compensated for a TE-polarized wave inside the structure. It is important to point out that although the loss is not fully compensated in the x direction, it is still lower than it would be without gain. To achieve loss compensation in both directions in this type of bi-layer metamaterial, we need an enormously large gain coefficient. It is also worth mentioning that the loss might be lower in real structures because the active medium within the metal-dielectric multilayer structure will give rise to an effective gain that is much higher than its bulk counterpart. The large value of gain is due to the local-field enhancement inherent in the plasmonic response of the structure [18].

In Fig. 4 we plot the incidence angle-dependent dispersion relationship of the silver-gain HMM. The incident wavelength is 720 nm. Here again we see perfect agreement between the NLE and SHA results. The results from EMT<sub>1</sub> do not show any dependence on the angle of incidence. The EMT<sub>2</sub> results show that this method can only handle angle-dependent problems in the y direction, and it has non-negligible error compared to the NLE or SHA results. As shown in Fig. 4, the permittivities in the x and y directions both show variations on the order of 1 in this case, which are rather strong changes. Thus, we should use either NLE or

SHA to take into account the angular dependence of the permittivity if we are dealing with angles away from normal incidence.

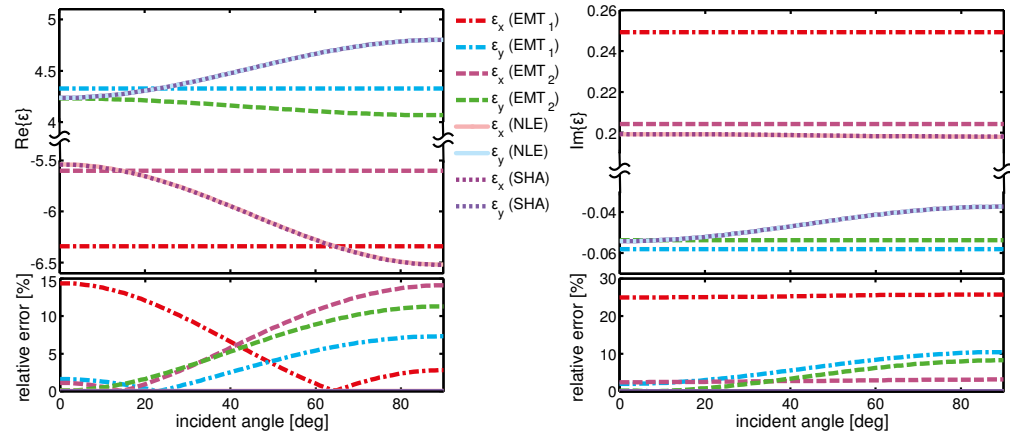


Fig. 4. Incidence-angle dependence of the effective anisotropic permittivity for the silver-gain HMM at a wavelength of 720 nm calculated from EMT<sub>1</sub> (dashed-dotted line), EMT<sub>2</sub> (dashed line), NLE (solid line), and SHA (dotted line). Top left panel: real part of the effective permittivity. Top right: imaginary part of effective permittivity. Bottom panels: relative errors in percent with respect to the SHA results. Note that the results from NLE and SHA are coincident, and their curves are overlapping.

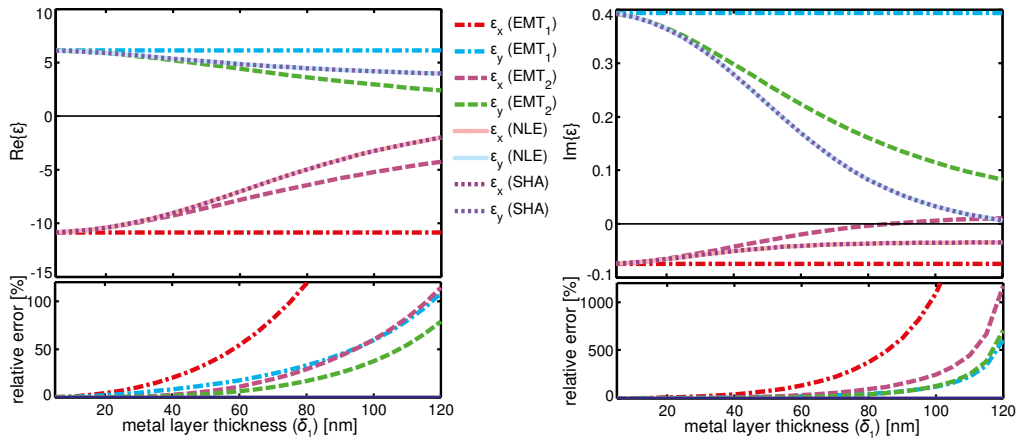


Fig. 5. Effective anisotropic permittivity for the silver-gain HMM with different metal-layer thicknesses at a wavelength of 720 nm at normal incidence ( $\theta = 0$ ) calculated from EMT<sub>1</sub> (dashed-dotted line), EMT<sub>2</sub> (dashed line), NLE (solid line), and SHA (dotted line). The volume fraction of the metal layer ( $\delta_1/\delta$ ) is kept constant at 0.5. Top left panel: real part of the effective permittivity. Top right: imaginary part of effective permittivity. Bottom panels: relative errors in percent with respect to the SHA results. Note that the results from NLE and SHA are coincident, and their curves are overlapping.

Our studies included an analysis of how the effective permittivity changes when varying the thicknesses of the metal layers. Figure 5 shows the calculated effective anisotropic permittivities when the metal-layer thickness varies from 5 nm to 120 nm. The metal volume fraction is kept constant at 0.5 (i.e.  $\delta_1 = \delta_2$ ). From the plotted curves, we can see that the results from NLE and SHA again show perfect agreement. The EMT<sub>1</sub> method does not have any thickness dependence at all, which also could be concluded from its formula. This method shows a significant amount of error when the metal-layer thickness is large. For instance, when the metal thickness reaches 60 nm (corresponding to a period of 120 nm, i.e.  $\lambda/6$ ), the

relative error for EMT<sub>1</sub> is greater than 50%. The EMT<sub>2</sub> method behaves slightly better, but the error also becomes non-negligible when the thickness increases.

We also investigated the calculated effective permittivity as a function of the metal volume fraction ( $\delta_1/\delta$ ). The period ( $\delta$ ) was kept constant at 60 nm in this case, and the results are shown in Fig. 6. As before, we again see that the NLE and SHA results match perfectly. For EMT<sub>1</sub> and EMT<sub>2</sub>, the results show that, in the x direction, the error increases as the metal volume fraction decreases. In the y direction, however, we see the opposite trend. We observe that, depending on the application, EMT<sub>1</sub> can produce substantial errors in both x and y directions of the effective dielectric function. The EMT<sub>2</sub> calculation gives more accurate results for major applications. The NLE and SHA methods are the most accurate for all the cases.

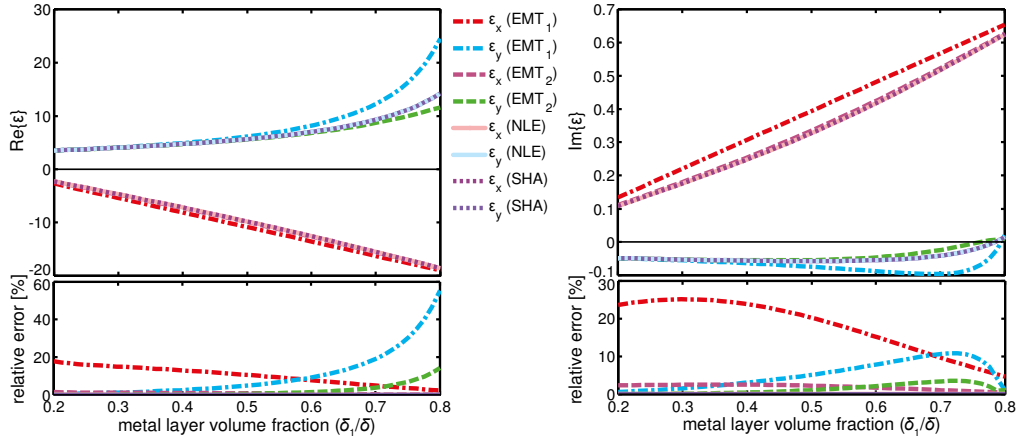


Fig. 6. Effective anisotropic permittivity for the silver-gain HMM with different metal volume fractions at a wavelength of 720 nm at normal incidence ( $\theta = 0$ ) calculated from EMT<sub>1</sub> (dashed-dotted line), EMT<sub>2</sub> (dashed line), NLE (solid line), and SHA (dotted line). The period ( $\delta$ ) is kept constant at 60 nm. Top left panel: real part of the effective permittivity. Top right: imaginary part of effective permittivity. Bottom panels: relative errors in percent with respect to the SHA results. Note that the results from NLE and SHA are coincident, and their curves are overlapping.

### 3. Applications

#### 3.1 Hypergratings

As shown above, lamellar metal-dielectric composite structures show typical hyperbolic dispersion. To utilize the unique properties of this metamaterial, one direct application is to use the structure for hypergratings [28]. A hypergrating is a device that combines a diffraction grating that can generate large-wavenumber modes and a planar slab of a hyperbolic metamaterial that can propagate those waves and let them converge at a subwavelength focal spot. A hypergrating is capable of producing subwavelength focal spots in a planar, non-resonant structure and is not limited to near-field operation. We show here an example of such a hypergrating using the lamellar metal-dielectric composite structure described above. The HMM slab consists of 30 layers of alternating 5-nm-thick silver layers and 18-nm-thick dyedoped epoxy layers. The size-dependent silver loss has been taken into account by setting the loss factor to two.

The effective anisotropic permittivities calculated for this design by NLE and SHA are shown in Fig. 7. At a wavelength of 716 nm, the effective permittivity in the x direction is about  $-3.05+0.14i$ , and in the y direction it is about  $3.59-0.049i$ , according to the SHA calculation. The loss has been over-compensated in the y direction and under-compensated in the x direction. As a source, we used a 100-nm-thick silver mask with two 20-nm-wide slits

spaced  $1\mu\text{m}$  apart on the top of the HMM slab. A plane wave at normal incidence and polarized perpendicular to the slits was sent in to the structure from the top. A schematic picture of the simulated structure is shown in Fig. 8(a). The electromagnetic field intensity map in the  $x$ - $y$  cross section of the structure at a wavelength of  $716\text{ nm}$  is shown in Fig. 8(b). The dashed line in the figure shows the approximate focal plane ( $345\text{ nm}$  deep into the surface of the HMM slab). The field intensity along the dashed line is shown in Fig. 8(c). We can clearly see that the electromagnetic field is transmitted through the slits and forms a subwavelength focal spot inside the HMM slab. With gain, the full width at half maximum (FWHM) of the field intensity on the focal plane is about  $43\text{ nm}$ , which is about  $\lambda/17$ . If there is no gain in the slab, the intensity at the focus is greatly reduced, and the FWHM of the field intensity increases to about  $50\text{ nm}$  as indicated by the dashed line in Fig. 8(c). The enhancements will be more prominent if a thicker HMM slab is used. Thus, by making the HMM structure active, we can improve the focusing performance of the hypergrating.

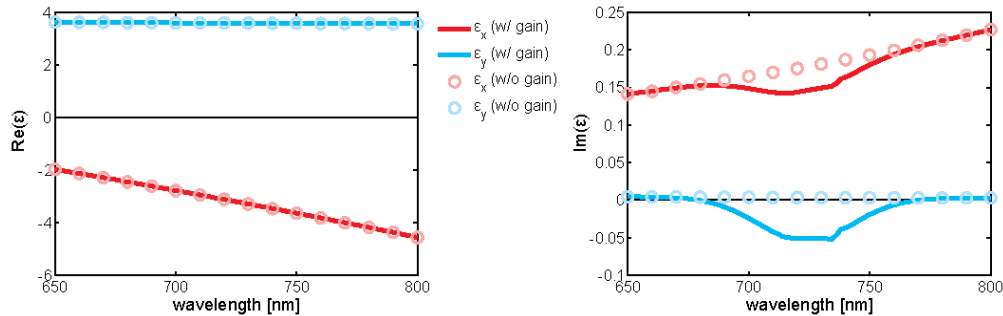


Fig. 7. Effective anisotropic permittivity calculated from NLE and SHA for a silver-dielectric HMM metamaterial with gain (solid line) and without gain (circles). Left panel: real part of permittivity. Right panel: imaginary part of permittivity.

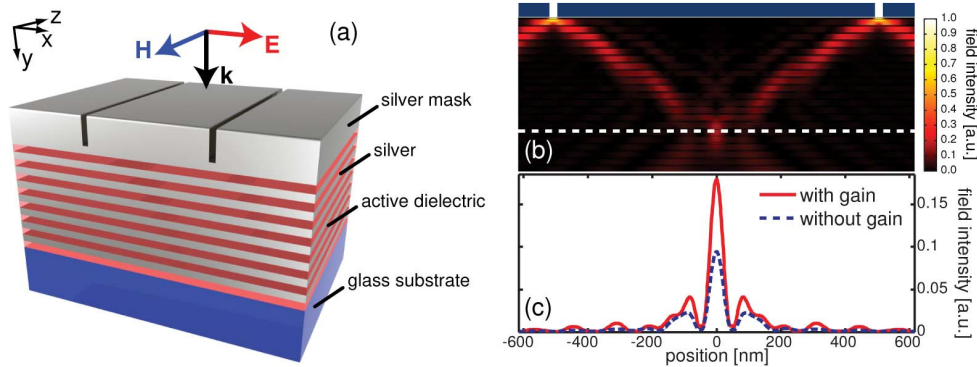


Fig. 8. (a) Schematic of the hypergrating structure. (b) Field intensity map plotted in the  $x$ - $y$  plane at a wavelength of  $716\text{ nm}$  with gain. (c) Field intensity plotted at a distance  $345\text{ nm}$  into the HMM slab with gain (solid line) and without gain (dashed line). The dashed line in (b) indicates the position of the cross section of (c).

### 3.2 Epsilon-near-zero (ENZ) materials

Another interesting application of this type of lamellar metal-dielectric composite metamaterial is an epsilon-near-zero (ENZ) material. By adjusting the metal and dielectric layer thicknesses to a certain ratio, the structure can display a very small real part of permittivity. The unique properties of ENZ materials enable exotic light behaviors. These materials are the subject of active research both in the linear [3, 4, 34] and nonlinear regimes [35–37]. If we again choose a dye-doped dielectric polymer as the dielectric layer and apply

the proper level of pumping, it is possible to obtain a loss-free ENZ material whose real and imaginary parts of permittivity will both be zero.

We demonstrate this kind of metamaterial using a lamellar metal-dielectric structure consisting of 100 layers of alternating 5-nm-thick silver layers and 45-nm-thick dye-doped epoxy layers. As usual, the size-dependent silver loss has been taken into account by setting the loss factor to two. The effective anisotropic permittivities calculated by NLE and SHA are shown in Fig. 9. We can clearly see that the real part of the permittivity in the x direction crosses zero at a wavelength around 730 nm. Note that the loss in the y direction has been over-compensated by the gain, while that in the x direction is under-compensated. In order to have a better understanding of the performance of the metamaterial, we simulated the structure using SHA with a plane wave incident in the y direction. In this case, the electric field will “feel” the permittivity in the x direction, so at a wavelength around 730 nm, it will “feel” zero permittivity. The transmittance, reflectance, and absorptance spectra calculated by SHA for this scenario are shown in Fig. 10(a).

Figure 10(b) shows the electric-field distribution along the propagation direction (from left to right) at a wavelength of 729 nm. Figure 10(c) shows the corresponding phase for the electric field. At this wavelength, the effective permittivity in the x direction is about  $0.02+0.04i$  with gain and  $0.02+0.07i$  without gain, according to the SHA calculation. Inside the multilayer slab, the phase of the electromagnetic field changes much more slowly inside the slab than outside the slab for several wavelengths. Note that inside an ideal ENZ material, the phase should be preserved, however, due to the residue of the effective permittivity (both real part and imaginary part), a small phase change still occurs. In addition, the homogenization process does not work well for the regions very close to the interface, and thus the phase changes more rapidly in those regions even though they are still inside the ENZ slab. Without gain (shown in the dashed lines of Fig. 10), the phase change slows down inside the ENZ, but very little intensity reaches the output. By introducing gain into the ENZ slab, the output intensity is 25 times stronger than in the no-gain case; moreover, the phase change is much smaller. Thus, by making the ENZ slab active, we can greatly increase the performance of the system.

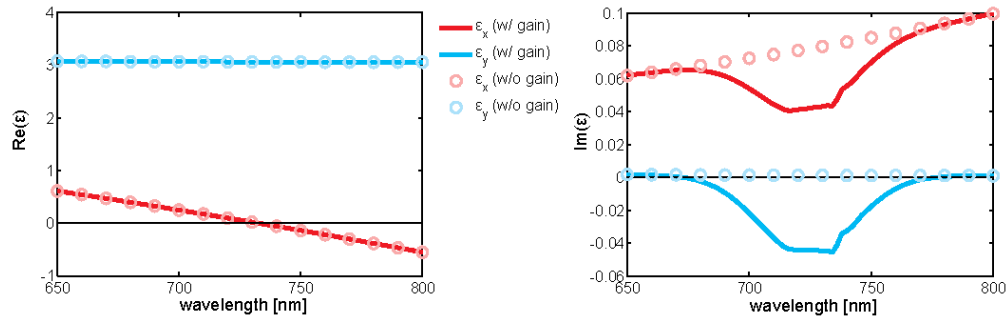


Fig. 9. Effective permittivity calculated from NLE and SHA for the silver-dielectric ENZ metamaterial with gain (solid line) and without gain (circles). (a) Real part and (b) imaginary part.

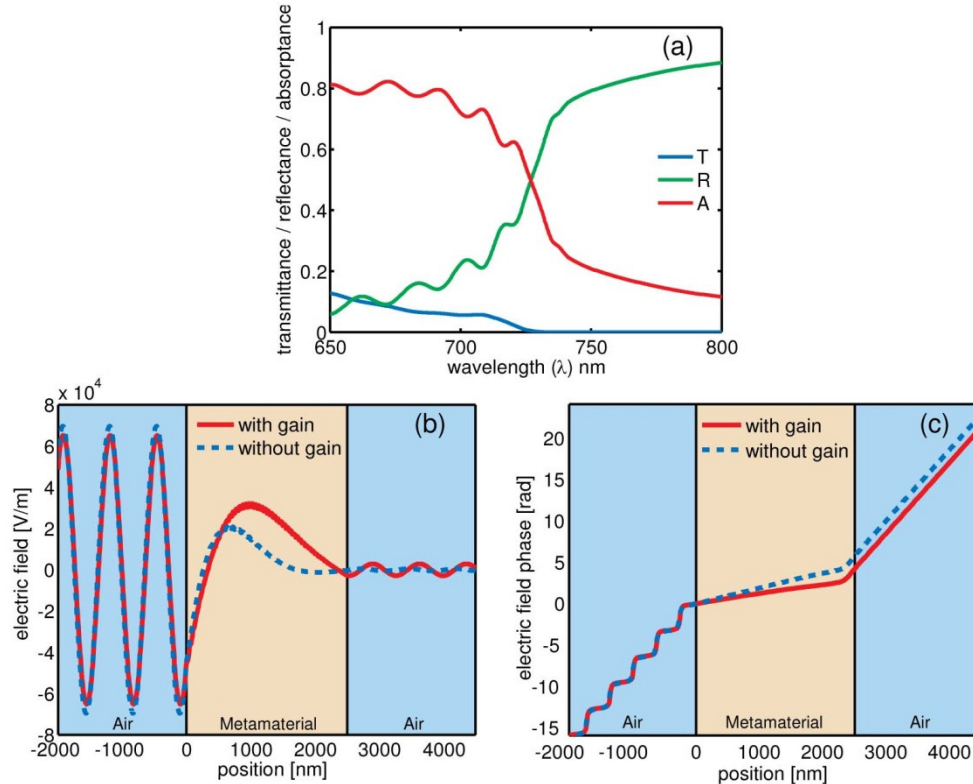


Fig. 10. (a) Transmittance, reflectance, and absorptance spectra calculated by SHA for a 100-layer silver-gain HMM with a silver-layer thickness of 5 nm and a gain-layer thickness of 45 nm. (b) Electric field and (c) the phase of the electric field plotted along the propagation direction at a wavelength of 729 nm with gain (solid line) and without gain (dashed line).

#### 4. Summary

In this paper, we have studied the dispersion relationships of metal-dielectric multilayer structures. We have focused on bi-layer structures of silver and a dye-doped dielectric polymer, and we studied the effective optical properties of the structure using the standard effective medium theory (EMT<sub>1</sub>) method, an angular-dependent nonlocal-effect-corrected EMT method (EMT<sub>2</sub>), a nonlinear equation-based eigenmode method (NLE), and a spatial harmonic analysis method (SHA). We showed that the effective permittivity resulting from NLE and SHA calculations are perfectly matched in both the x and y directions of the structure and for all cases we considered. Since both of these methods focus on calculating the eigenvalues of the composite layer and differ only in their numerical realizations, they give highly accurate results provided that a sufficiently large system matrix is used for diagonalization in SHA [26].

The results from the EMT<sub>2</sub> method are very close to those of NLE and SHA for most cases, and for some applications EMT<sub>2</sub> has error values that are less than 3%. Overall, though, EMT<sub>2</sub> does show some observable error, and with oblique incidence, EMT<sub>2</sub> exhibits significant error values. The method also gives non-negligible error values when the layers are thick or when the metal-to-dielectric thickness ratio is large.

There are significant discrepancies between the results from the simple EMT<sub>1</sub> method and those from the other methods. We observed that, depending on the application, EMT<sub>1</sub> can produce substantial errors in both the active and lossy directions of the effective dielectric function. Since EMT<sub>1</sub> does not exhibit any dependence on the layer thicknesses at all, it

shows a significant amount of error when the thicknesses are large. For instance, when the metal thickness is about  $\lambda/12$ , the relative error for  $\text{EMT}_1$  is greater than 50%. In addition, the imaginary parts of the permittivities from both  $\text{EMT}_1$  and  $\text{EMT}_2$  are higher in the active region of the spectrum.

Our study also shows that when the dye is completely saturated, the silver-gain binary lamellar structure becomes loss-free in the direction perpendicular to the layers (the x direction in our definition). However, it is much more difficult to compensate the metal loss in the direction parallel to the layers (the y direction in our definition). Doing so requires a huge gain coefficient in the active medium, which is not easy to obtain in real experiments.

Multilayer structures that exhibit hyperbolic dispersion are desirable for a number of applications, including superlenses, hyperlenses and quantum optical devices. In this work, we have shown two realizable examples of applications of hyperbolic, multilayer structures with gain, i.e., a hypergrating and an ENZ metamaterial. We compared the behaviors of these devices with and without gain, and we showed that by introducing gain into such structures, the performance will improve greatly.

## 5. Addendum

In this section we show the details of the four different methods that we used to model a binary planar HMM, i.e., a lamellar metal-dielectric composite consisting of only two different types of isotropic layers. The geometry is defined in Fig. 1.

### 5.1 Nonlinear equation (NLE) method

It is known that the permittivity values calculated from the standard effective medium theory (EMT) can deviate from the exact solutions [6, 25]. To obtain a rigorous analytical solution for our study, we used the T-matrix approach [38]. (In contrast with [38], the time-dependent factor  $\exp(-i\omega t)$  is taken here). We arrive at nonlinear equations for the transverse electric field (TE) polarization in which the incident electric field only has a z component

$$\cosh(g_2\delta_2)\cosh(g_1\delta_1) + \frac{1}{2}\left(\frac{g_1}{g_2} + \frac{g_2}{g_1}\right)\sinh(g_2\delta_2)\sinh(g_1\delta_1) = \cosh(\alpha\delta + i2\pi q) \quad (1)$$

and for the transverse magnetic field (TM) polarization in which the incident magnetic field only has a z component

$$\cosh(g_2\delta_2)\cosh(g_1\delta_1) + \frac{1}{2}\left(\frac{g_1\varepsilon_2}{g_2\varepsilon_1} + \frac{g_2\varepsilon_1}{g_1\varepsilon_2}\right)\sinh(g_2\delta_2)\sinh(g_1\delta_1) = \cosh(\alpha\delta + i2\pi q), \quad (2)$$

where  $g_1$  and  $g_2$  are the wavenumbers in y direction for layer 1 and layer 2, respectively.

For the TE polarization

$$\begin{aligned} g_1 &= \sqrt{k_{x,\text{TE}}^2 - \varepsilon_1 k_0^2} \\ g_2 &= \sqrt{k_{x,\text{TE}}^2 - \varepsilon_2 k_0^2}, \end{aligned} \quad (3)$$

and for the TM polarization

$$\begin{aligned} g_1 &= \sqrt{k_{x,\text{TM}}^2 - \varepsilon_1 k_0^2} \\ g_2 &= \sqrt{k_{x,\text{TM}}^2 - \varepsilon_2 k_0^2}, \end{aligned} \quad (4)$$

where  $q \in \mathbb{Z}$ ,  $\iota = \sqrt{-1}$ , and  $\alpha = ik_0 \sin \theta$ .

Since the eigenvalue  $k_x$  in the x direction is preserved across all interfaces, the effective permittivities are  $\tilde{\varepsilon}_x = k_{x,TE}^2/k_0^2$  and  $\tilde{\varepsilon}_y = k_{x,TM}^2/k_0^2$ , where  $k_{x,TE}$  and  $k_{x,TM}$  are the eigenvalues that can be obtained by solving the system of non-linear equations given in Eqs. (1) and (2).

### 5.2 Effective medium theory (EMT<sub>1</sub>) method

To understand the electromagnetic properties of metal-dielectric multilayers, the standard EMT is a simple and useful method. We denote this method as EMT<sub>1</sub>. A plane wave inside an effective medium obeys the standard dispersion relation

$$\frac{k_x^2}{\varepsilon_y} + \frac{k_y^2}{\varepsilon_x} = k_0^2, \quad (5)$$

with  $k_y = k_0 \sin \theta + 2\pi q/\delta$ , and where  $q \in \mathbb{Z}$  is the diffraction order.

We now expand  $\cosh(g_j \delta_j)$  and  $\sinh(g_j \delta_j)$ ,  $j=1,2$  in (1) for  $g_j \delta_j \ll 1$ , and, after dividing both parts by  $\delta^2$  and keeping the results up to quadratic terms, we arrive at

$$g_1^2 r^2 + g_2^2 (1-r)^2 + r(1-r) \left( g_1^2 \frac{\varepsilon_2}{\varepsilon_1} + g_2^2 \frac{\varepsilon_1}{\varepsilon_2} \right) = -k_y^2. \quad (6)$$

Here  $r = \delta_1/\delta$  is the volume fraction of the metal layer. Then, using  $g_j^2 = k_x^2 - \varepsilon_j k_0^2$ ,  $j=1,2$  and comparing the result to Eq. (5), we have

$$k_x^2 \underbrace{\left[ r\varepsilon_1^{-1} + (1-r)\varepsilon_2^{-1} \right]}_{\varepsilon_y^{-1}} + \frac{k_y^2}{\underbrace{r\varepsilon_1 + (1-r)\varepsilon_2}_{\varepsilon_x}} = k_0^2. \quad (7)$$

Hence, the effective permittivities in the directions parallel ( $\varepsilon_x$ ) and perpendicular ( $\varepsilon_y$ ) to the thickness direction are

$$\begin{aligned} \varepsilon_x &= r\varepsilon_1 + (1-r)\varepsilon_2 \\ \varepsilon_y^{-1} &= r\varepsilon_1^{-1} + (1-r)\varepsilon_2^{-1}. \end{aligned} \quad (8)$$

It is obvious that Eq. (8) neglects any angular dependence and is denoted here as EMT<sub>1</sub>. The beauty of EMT<sub>1</sub> is that it is simple and can be easily used for initial designs. For example, supposing that we know the desired effective permittivity components  $\varepsilon_x$  and  $\varepsilon_y$ , we can obtain the permittivities of the constituent materials in the metamaterial by using

$$\begin{aligned} \varepsilon_1 &= \frac{\varepsilon_x - \varepsilon_y \mp \sqrt{(\varepsilon_x - \varepsilon_y)(4r(1-r)\varepsilon_y + \varepsilon_x - \varepsilon_y)} + 2r\varepsilon_y}{2r}, \\ \varepsilon_2 &= \frac{\varepsilon_x + \varepsilon_y \pm \sqrt{(\varepsilon_x - \varepsilon_y)(4r(1-r)\varepsilon_y + \varepsilon_x - \varepsilon_y)} + 2r\varepsilon_y}{2(1-r)}. \end{aligned} \quad (9)$$

In principle, both solutions can be used to form a multilayer structure having the designated effective permittivity. In practice, one should also take into account the availability of the elemental constituent materials in nature.

### 5.3 Angular-dependent effective medium theory (EMT<sub>2</sub>) method

We can also consider a modification to the standard EMT method that takes non-local effects into account. We denote this method as EMT<sub>2</sub>. We begin with the set of equations [25]

$$\begin{aligned}\hat{\varepsilon}_x &= \varepsilon_x (1 - \Delta_x)^{-1} \\ \hat{\varepsilon}_y &= \varepsilon_y (1 - \Delta_y)^{-1},\end{aligned}\tag{10}$$

which account for non-local effects including angular dependence. In Eq. (10),

$$\begin{aligned}\Delta_x &= \frac{1}{12} \delta^2 r^2 (1-r)^2 (\varepsilon_1 - \varepsilon_2)^2 / \varepsilon_x \\ \Delta_y &= \Delta_x \left( \frac{\varepsilon_y^2 \varepsilon_x^2}{\varepsilon_1^2 \varepsilon_2^2} - \alpha^2 (\varepsilon_1^{-1} + \varepsilon_2^{-1})^2 \varepsilon_y^2 / \varepsilon_x \right).\end{aligned}\tag{11}$$

The rest of the analysis closely follows that of the EMT<sub>1</sub> method and is not repeated here.

#### 5.4 Spatial harmonic analysis (SHA) method

The spatial harmonic analysis (SHA) method, also known as the Fourier modal method (FMM) or rigorous coupled wave analysis (RCWA), is one of the most widely used methods based on differential equations for studying the diffraction characteristics of electromagnetic waves in periodic structures. The advantages of SHA are that it is a non-iterative and mesh-free technique for obtaining the exact solution to Maxwell's equations using the Bloch-Floquet formalism. Recent publications show that the SHA method has been successfully used to simulate plasmonic structures and metamaterials [26, 27, 39]. We modeled the multilayer structure with a two-dimensional SHA in a single layer (each layer in the structure is a segment in the model) with arbitrary thickness, and we extracted the dominant eigenmode obtained by SHA. We get the effective dielectric permittivity from the wavevector of the eigenmode. Note that the two-dimensional version of SHA is staged online and is free for public access [40].

#### Acknowledgment

This work was supported in part by Samsung Advanced Institute of Technology, ARO MURI Awards 50342-PH-MUR and W911NF-09-1-0539, ONR MURI grant N00014-10-1-0942, and Intelligence Community Postdoctoral Research Fellowship Grant #104796.